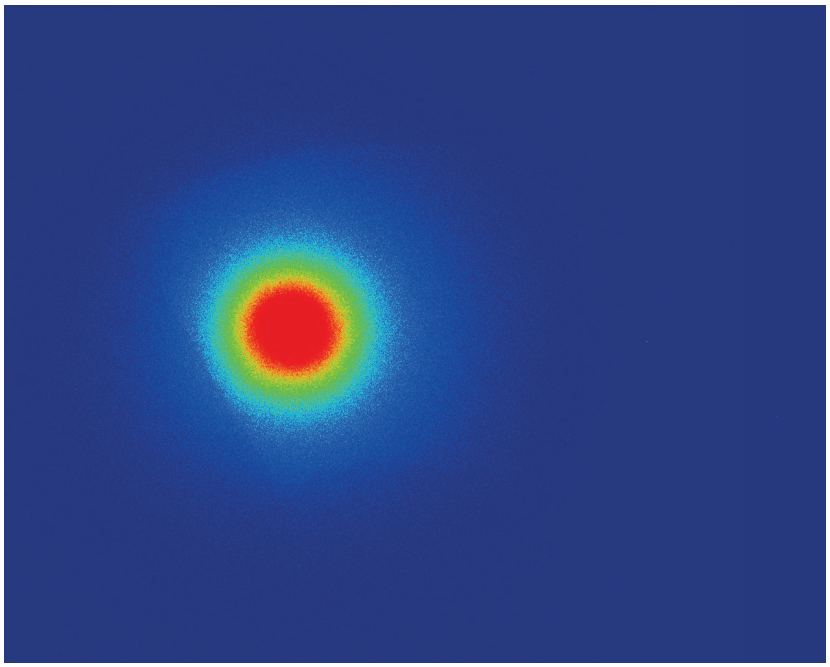

Sampling and evaluation of in-situ studies for ^{60}Co diffusion in bentonite

Master's thesis in Nuclear Science and Technology

MIKAEL BECKIUS

Department of Nuclear Chemistry
CHALMERS UNIVERSITY OF TECHNOLOGY
Gothenburg, Sweden 2020

Master's thesis 2020:KBTX12

Sampling and evaluation of in-situ studies for ^{60}Co diffusion in bentonite

Mikael Beckius

CHALMERS
UNIVERSITY OF TECHNOLOGY

Chemistry and Chemical Engineering
Nuclear Chemistry
Chalmers University of Technology
Gothenburg, Sweden 2020

Sampling and evaluation of in-situ studies for ^{60}Co diffusion in bentonite
MIKAEL BECKIUS - mikbec@student.chalmers.se

Supervisors: Stellan Holgersson, Department of Chemistry & Chemical Engineering,
Patrik Sellin, Svensk Kärnbränslehantering AB
Examiner: Christian Ekberg, Department of Chemistry & Chemical Engineering

Master's Thesis 2020:KBTX12
Department of Chemistry & Chemical Engineering
Division of Nuclear Chemistry
Chalmers University of Technology
SE-412 96 Gothenburg
Telephone +46 31 772 1000

All images are created by myself unless stated otherwise.
Cover: Autoradiogram showing one of the laminae containing radioactive tracer.

Typeset in LaTeX
Printed by Chalmers Reproservice
Gothenburg, Sweden 2020

Sampling and evaluation of in-situ studies for ^{60}Co diffusion in bentonite

MIKAEL BECKIUS
Department of Chemistry & Chemical Engineering
Chalmers University of Technology

Abstract

This study focuses on evaluating the diffusion of ^{60}Co in bentonite clay as part of an in-situ experiment made by SKB at Äspö. This experiment has been running for 20 years, and its purpose is to evaluate the potential of using bentonite clay as backfill material in a final repository for used nuclear fuel. Evaluating the diffusivity is one method of assessing the long-term structural integrity of the bentonite clay. This is done by using ^{60}Co as a radioactive tracer placed in a block of bentonite inside a test parcel designed to mimic the proposed setup of the Swedish KBS-3 final repository model. This specific setup is under adverse conditions where the temperature is higher than the estimated temperature in the final repository. This is done to obtain a comparison with previous studies done under normal conditions. The bentonite around the radioactive source is sampled and crushed before the radioactivity is measured using an HPGe detector with sample changer. The calculated diffusivity is used to evaluate whether the diffusion model used in earlier studies is applicable on this test parcel as well.

The results obtained in this study, shown in Table 0.1, supports earlier studies, as the calculated diffusivity fits well into the diffusion model and yields a diffusivity within an order of magnitude from the results obtained in earlier studies for the fast profiles, and in line with earlier results for the slow profiles. Combining this result with the previous studies on the subject show that the bentonite structure appears to be intact, which further supports the idea that bentonite clay is a very promising material for use as backfill material in a final repository.

Table 0.1: Apparent diffusivity of ^{60}Co in three different isotherms

Name	$\mathbf{D}_a$ **[m^2/s]**	**T [^{o}C]**
Isotherm 2 (fast)	$8.78{\cdot}10^{-13}$	81
Isotherm 2 (slow)	$9.61{\cdot}10^{-14}$	81
Isotherm 3 (fast)	$3.44{\cdot}10^{-13}$	75
Isotherm 3 (slow)	$6.75{\cdot}10^{-14}$	75
Isotherm 4 (fast)	$2.17{\cdot}10^{-13}$	69
Isotherm 4 (slow)	$7.19{\cdot}10^{-14}$	69

Keywords: bentonite, diffusion, cobalt, nuclear fuel, final repository, SKB.

Acknowledgements

Stellan Holgersson, for invaluable support throughout the work, both in the lab and providing his extensive knowledge whenever needed.

Patrik Sellin, for support and insight in SKB and their experiments.

Magnus Kronberg, for providing pictures, figures, reports and making sure the samples were delivered to the lab. Also for making an interesting study visit at the Äspö Hard Rock Laboratory possible.

Stefan Allard, for all help with the autoradiography, as well as making sure the experimental part was carried out in a safe and orderly fashion.

I would also like to thank everyone at the Nuclear Chemistry and Industrial Metal Recycling department for making me feel part of the team, always taking time to answer my questions and also all the crossword sessions during fika and lunch breaks. This work wouldn't have been nearly as joyous without you.
A special mention also goes out to my cousin Gustav Palm, who was of great help in making illustrations for this work.

Mikael Beckius, Gothenburg, September 2020

Contents

Glossary

Abbreviations

BWR	Boiling Water Reactor
GCR	Gas-cooled Reactor
HPGe	High Purity Germanium, detector type for γ-radiation
KBS-3	The model for storing used nuclear fuel proposed by SKB
LOT	Long-term studies of buffer materials carried out by SKB
LWGR	Light Water-cooled Graphite-moderated Reactor
PHWR	Pressurised Heavy Water Reactor
PWR	Pressurised Water Reactor
SKB	Svensk Kärnbränslehantering AB, the authority responsible for handling used nuclear fuel in Sweden

Glossary

Bentonite	A clay mineral that swells when coming in contact with water
Diffusion	A physical phenomena occuring in a system with a concentration gradient
Final Repository	Final storage of used nuclear fuel, often in bedrock
Fissile	A nucleus that has a high probability of undergoing fission when interacting with an incoming neutron
In-situ	Experiment carried out on-site
Moderator	Material that slows down neutrons inside a reactor, typically water (H_2O), heavy water (D_2O) or graphite
Nucleus	The inner part of an atom, consisting of protons and neutrons

List of Figures

List of Tables

1

Introduction

1.1 Aim

The aim of this study is to do an *in-situ* evaluation of the diffusion of the radionuclide ^{60}Co in bentonite clay. This is done as a part of an experiment carried out by Svensk Kärnbränslehantering AB, *SKB*, in order to evaluate the bentonite clay, a material in the multi-barrier system proposed for the final repository of spent nuclear fuel.

1.2 Problem description

Used nuclear fuel mostly consists of highly radioactive isotopes of different elements, meaning they are harmful due to the emitted radiation that causes damage to DNA and other parts of the living cell division mechanisms. It is therefore vital to ensure that there will be no exposure to any living organisms or the environment of these radioactive elements. There are no operational final repositories for spent nuclear fuel in the world today, only intermediate storage and storage of short-lived radioactive waste. Due to the complexity of the technical problems that must be solved, this is a field of research that has been going on for several decades, but not on a practical scale until quite recently. Still, there are many technical challenges and associated problems, both known and unknown left to tackle in order to construct an operational final repository, which is the ultimate goal of the research that is carried out by SKB in Sweden.

1.3 Scope

This thesis is focused on analysing the diffusion of ^{60}Co in bentonite clay from a particular *in-situ* experiment at Äspö Hard Rock Laboratory, near Oskarshamn. However, several other experiments are carried out inside the same test parcel, such as copper corrosion and hydraulic effects. These will not be included in the thesis, since they are being carried out on-site at SKB or at laboratories specialising in the required analysis methods.

1.4 Background

1.4.1 Nuclear Power

In the late 1930s, Lise Meitner and Otto Hahn discovered that certain heavy atom nuclei could be split into two new, lighter nuclei by bombarding it with neutrons, a reaction called fission. [1] This reaction also released a significant amount of energy in the process due to a tiny mass difference between the original nucleus and the two new nuclei, the Δm, in the famous equation

$$E = \Delta m c^2 \tag{1.1}$$

where E is the energy released, and c is the speed of light in vacuum. Almost immediately, several laboratories around the world started to replicate the experiments carried out by Hahn and Meitner, with the goal to observe and potentially even harness the energy released. In 1942 Enrico Fermi built the Chicago-Pile 1, where the first self-sustaining nuclear chain reaction took place, a major breakthrough in the field of nuclear science. The first nuclear reactor designed for creating electricity was started at the Argonne National Laboratory, USA in 1951, the first completely civilian nuclear power station was started at Calder Hall, England in 1956.

Since those first steps were made the nuclear industry initially developed quickly. However, after the light water reactors were established, the development stagnated with few new systems being added. The most significant changes were made after incidents or accidents that occurred due to lack of knowledge of different conditions that may arise inside a reactor, and therefore the required safety systems were either faulty or not in place. Now there are several up- and coming projects that look into the so called Generation IV systems, where loss-of-coolant accidents (Harrisburg, Fukushima) or excessive reactivity accidents (Chernobyl), are made impossible by the inherent design of the reactor. In some of these reactor designs, the used nuclear fuel is to be recycled and reprocessed into new fuel that can be used inside the new reactor, making use of approximately 90-98% of the energy inside the fuel, as compared to the 5% that is used in reactors today before being sent for storing and ultimately a final repository.

Today there are 447 nuclear reactors in operation, with another 52 under construction, amounting to approximately 10% of the total electricity produced globally. [2] This is a significant amount, but the nuclear sector of electricity production still pales in comparison with the 38% of the total electricity being produced by fossil fuels such as coal, oil and gas, which contribute a large part of the CO_2-emissions globally making nuclear an important sector to look at in order to combat climate change.

There are a few main types of reactors in operation (PWR, BWR, PHWR, GCR, LWGR), but the main principle is the same for all of them; the nuclear fuel which consists of around 2-5% of enriched uranium (^{235}U, which is fissile) is placed in rods in the reactor core. Inside the reactor core is also the control rods which are

used to control the nuclear chain reaction by absorbing some of the neutrons. In order for the chain reaction to start, the spontaneous fission inside the fuel is not producing a sufficient amount of neutrons, so a neutron source is introduced into the core to induce nuclear reactions. The reactor core also contains a moderator, whose purpose is to slow the neutrons down to make interaction between neutron and fuel easier, increasing the probability of a fission reaction. The most common moderator is water (used in BWR and PWR), but there are some types of reactors that use either heavy water (D_2O, used in PHWR) or graphite (used in LWGR and GCR). The water is also a coolant and flows through the core and it is heated by the released energy. The heat is transferred either directly by boiling (Boiling water reactor, BWR), or fed to a steam generator where a secondary water flow is heated to boiling (Pressurised water reactor, PWR), the steam is then fed to large turbines, which drive generators that are producing electricity to the grid. In a GCR, the coolant is CO_2 gas that heats the steam generators.

The lighter nuclei formed by the nuclear fission reactions are predominantly radioactive with highly varied half-lives, while not being fissile themselves. This means that after some time the fuel must be replaced, and the remains of the used fuel needs to be cooled and stored until the radioactivity has decreased to a safe level. As shown in Figure 1.1, this takes approximately 4-500 years years for the fission products, and up to 100 000 years for the heavier actinides. [3]

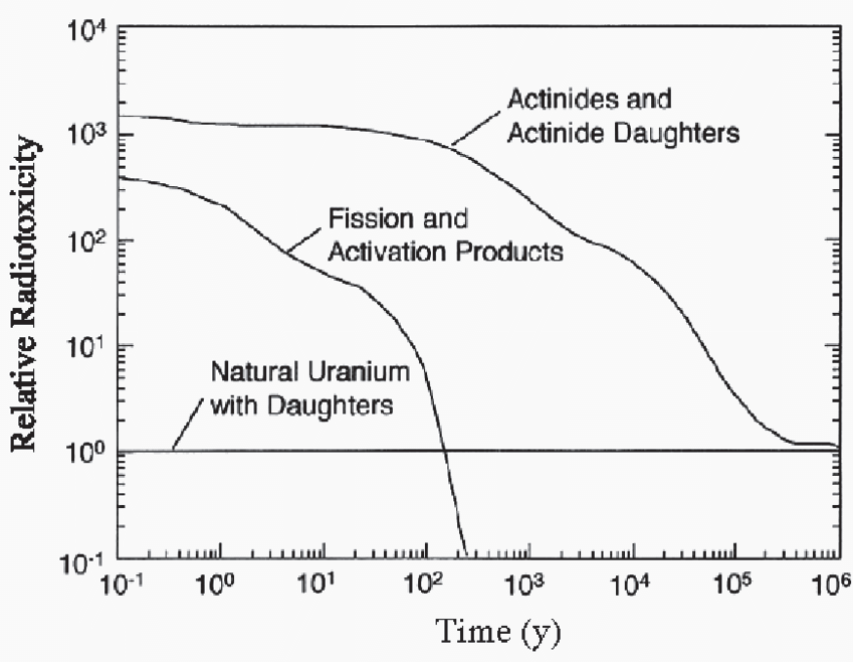

Figure 1.1: Graph showing radiotoxicity in used nuclear fuel [3]

1.4.2 SKB and LOT-experiments

The Long Term Test of buffer materials, LOT, are among the oldest experiments carried out at the Äspö laboratory at Svensk Kärnbränslehantering AB, *SKB*. The SKB company is responsible for the handling and storing of spent nuclear fuel in Sweden. The purpose of the studies carried out by SKB is to examine and evaluate methods for constructing a final repository that is safe for storing the used nuclear fuel from the Swedish nuclear power plant. The repository is intended to stay intact for the projected time of up to 100 000 years when the radioactivity is expected to be no higher than the background activity in the bedrock. [4] The Äspö underground laboratory near Oskarshamn was opened in 1995 for the purpose of providing possibilities for full-scale research related to a final repository of used nuclear fuel.

The test setup, illustrated in Figure 1.2, consists of a 4700 mm long copper tube with an inner diameter of 100mm which is surrounded by pre-compacted blocks of bentonite clay resulting in an outer diameter of 700 mm. The copper tube was fitted with a heater in order to simulate the decay heat from the radionuclides in the spent fuel. Inside the bentonite are several thermocouples, humidity and pressure gauges to monitor the temperature and water saturation evolution during the experiment.

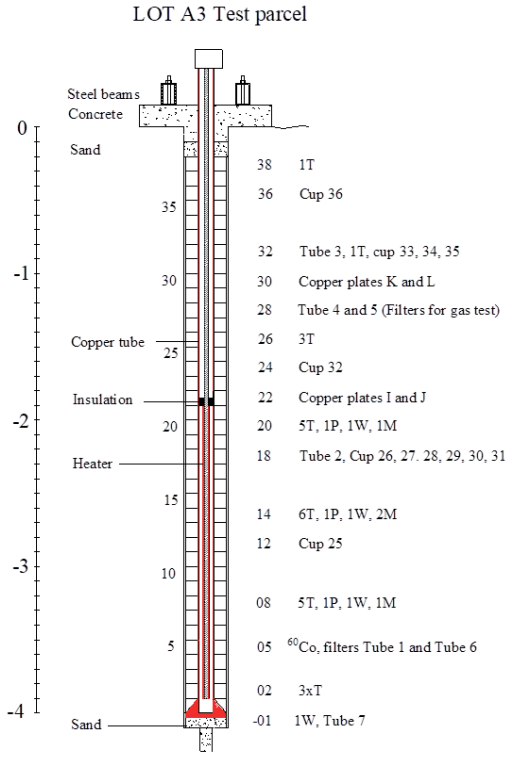

Figure 1.2: Illustration of test package A3 [5]

Two very small (radius 2mm) bentonite plugs were ion-exchanged to each contain

1MBq of the radionuclide ^{60}Co and inserted diametrically opposite each other in the third block from the bottom. This was done in order to evaluate the diffusion of radionuclides inside the bentonite clay. Several other experiments are carried out in the bentonite blocks over the length of the copper tube, among them copper plates to study corrosion effects during repository conditions. The installed heater maintains a temperature at the surface of the copper tube at 90 ^{o}C in the standard parcels, and 130 ^{o}C in the tests that are designed to study adverse conditions, which is the case for this study. In total seven test parcels were installed, three with standard conditions and four with adverse conditions. These parcels are divided into short-term (1-2 years) tests, medium term (>5 years) tests and long-term (>10 years) tests with at least one standard and one adverse parcel in each test.

The test parcels were installed into vertical holes drilled into the bedrock in a gallery Äspö tunnel at approximately 450m below sea level. The holes were filled up with approximately 10cm of sand at the bottom, and the hole was sealed off with a concrete plug. The installation of test parcel A3 was done together with several other similar parcels in 1999, before being disassembled for analysis and evaluation in 2019.

The proposal from SKB, named KBS-3, for the different barriers is illustrated in Figure 1.3, where the first barrier is the cladding of a single fuel pin, which consists of Zircaloy, an alloy of lighter metals such as zirconium and tin, nickel and iron. Several of these fuel pins are placed inside a cast iron insert which in turn is placed inside a copper canister that is welded shut. This copper canister is lowered into vertical bore holes inside the bedrock, and rings of compacted bentonite clay is used as backfill material between the canister and the bedrock. These holes are approximately 400-500 meters under the surface, meaning that the bedrock is the last barrier preventing radioactive materials from escaping the final repository [4].

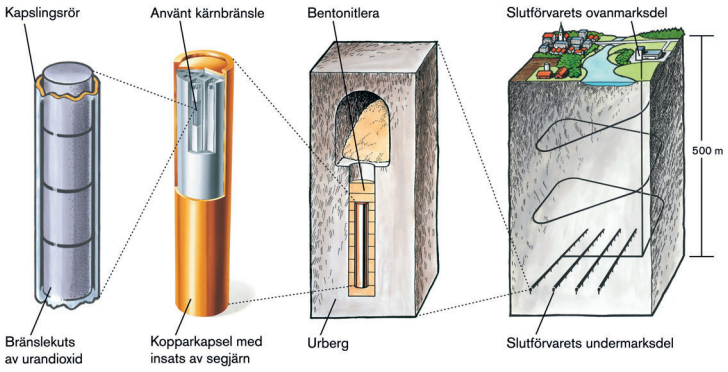

Figure 1.3: Illustration of the barriers inside the final repository [5]

2

Theoretical

2.1 Bentonite

Bentonite is a clay material that is mainly made up of smectite type minerals, a group of minerals characterised by hydrous aluminium silicates containing iron and magnesium, and either sodium or calcium. Depending on whether sodium or calcium is present, the bentonite has different characteristics; in the case of sodium it can absorb large amounts of water, while swelling to several times the initial volume in the process. The bentonite containing calcium doesn't swell like the sodium containing one, instead it forms a granulate that's highly absorbent, called "Fuller's earth". [6]

This ability to swell and also effectively sorb cations make bentonite the most promising backfill material in a future final repository for spent nuclear fuel, as the possibility for radionuclides from the fuel do diffuse through the bentonite is severely hindered as studies by Triantafyllou et. al. and Xu et. al. shows. [7] [8] This is also supported by several studies at SKB on bentonite as backfill material. [5] [9] The sodium containing bentonite has become a material with many different uses due to the swelling properties. Some examples are as sealing landfills to ensure no leakage of toxic or dangerous substances, as drilling mud, as filler in cements. This also makes it useful as backfill material in the proposed final repository, since the swelling that occurs after the clay has been saturated by groundwater slows down the diffusion processes that may occur around the deposited fuel canister. [6]

2.2 Diffusion

Diffusion is a phenomena that occurs when a system contains a medium with a dissolved component with a varying concentration. This will cause material from the high concentration areas of a component to migrate by Brownian motion towards low concentration areas of the same component in order to even out the concentration gradient. This phenomena is present in many biological mechanisms, for example ion transport through cell membranes, as well as chemical processes like separation operations. [10]

A study by Appelo shows that there are three types of diffusion processes inside bentonite clay; free water diffusion between the mineral layers, pore diffusion through the mineral layers and a diffuse double layer at the boundary between the mineral layers and the free water. [11] This has to be taken into account when calculating the diffusivity through the mineral structure. Appelo also describes in more detail what the diffusion phenomena looks like as well as the distribution of anions and cations, the latter being the most important for this work since Co forms the Co^{2+} cation in water. In Figure 2.1 the different diffusion modes can be seen, where 1 is the intraparticle diffusion, 2 is the boundary layer and 3 is the interparticle diffusion in the free porewater. TOT in the figure denotes the tetrahedral-octahedral-tetrahedral structural layers of aluminosilicates, where the negative charge on oxygen atoms are balanced by the exchangeable cations in the interlayer space.

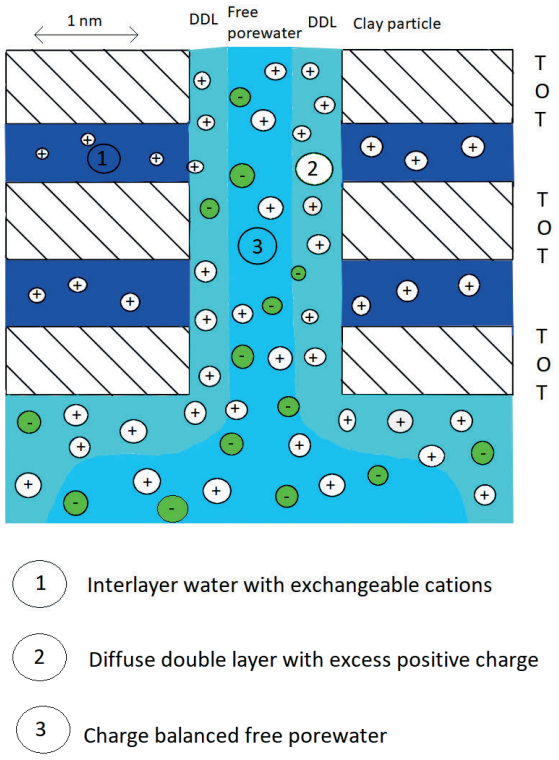

Figure 2.1: Diffusion of cations through bentonite clay

In order to study the diffusion process through a media, a tracer is often used. This tracer can be either a dye in a liquid, or as in this case, a radioactive element

which is distinguishable from the diffusing component whilst still having the same characteristics to ensure it behaves like the diffusing component. In this study the radionuclide used is ^{60}Co, a radioactive isotope of cobalt which has a half-life of 5.2 years, and two distinct and easily identifiable γ-peaks. This makes it a good choice for this kind of long-term studies since it's decay is slow enough to monitor processes during long time periods, but still short enough to have significant activity.

In the evaluation of the diffusion data, the model that will be used is based on a solution for Fick's 2nd law of diffusion for the diffusion of a finite source into an infinite medium. If one assumes the source to be spherical with diameter a, and the initial concentration is C_0, the concentration C at time t and radius r, C(r,t), is given by equation 2.1 [12]

$$C(r,t) = \frac{1}{2}C_0\Big[erf\frac{a+r}{2\sqrt{D_a t}} + erf\frac{a-r}{2\sqrt{D_a t}}\Big] - \frac{C_0}{r}\sqrt{(\frac{D_a t}{\pi})}\Big[e^{\frac{-(a-r)^2}{4Dt}} - e^{\frac{-(a+r)^2}{4Dt}}\Big] \quad (2.1)$$

where D_a is the apparent diffusivity and *erf* is the error function given by Equation 2.2

$$erfz = \frac{2}{\sqrt{\pi}}\int_0^z e^{-t^2}dt \quad (2.2)$$

The diffusion of Co in bentonite has been studied before, both at SKB, such as the CHEMLAB trace experiments by Jansson, which showed that Co-ions readily sorb onto the bentonite at pH levels of 6.5 to 8.5, as well as several studies by Karnland [13] [5] [9]. A study on migration of heavy metal ions and the use of bentonite as backfill material by Triantafyllou et al. [7] shows that complexation on the surface contribute to the slow diffusion of Co. These are results that are further supported by sorption studies carried out by Xu et. al. [8]. The work by Molera and Marimon shows that Co-ions have low diffusivity in bentonite, and are immobilized upon sorption. [14]. Some results from the previous diffusion studies on Co in bentonite clay and their respective temperature are shown in Table 2.1. It should be noted that the study by Eriksen and Nilsson is done on a similar LOT-test parcel under adverse conditions, however the test period used in that study was medium-term, meaning that the test parcel was unearthed 6 years after the experiment started. [5]

Table 2.1: Previous studies on the diffusion of Co in bentonite clay

Study	**Temperature [^{o}C]**	**D_a [m^2/s]**
Jansson et. al. [13]	20	$(2\pm1)\cdot10^{-14}$
Jansson et. al.[13]	70	$8\cdot10^{-14}$
Jansson et. al.[13]	90	$1.2\cdot10^{-13}$
Karnland et. al. [9]	90	$2\cdot10^{-13}$
Eriksen, Nilsson [5]	95	$5\cdot10^{-13}$
Molera, Marimon [14]	20	$3\cdot10^{-14}$

2.3 Radionuclide

A radionuclide is a radioactive isotope of a chemical element, i.e it has a set number of protons in it's nucleus, but the number of neutrons may vary. Since the number of protons is the same, the element keeps its chemical properties, but increasing or decreasing the number of neutrons may cause instability in the nucleus. This causes the nucleus to decay, where one or more particles are emitted in order to become stable.

There are three main modes of decay, α-decay where a He-nucleus consisting of 2 protons and 2 neutrons is emitted, β-decay where an electron or positron is emitted, depending on whether there are too many or too few neutrons compared to the stable isotopes of the elements. The third mode of decay is γ-decay, which occurs after α- or β-decay, and the resulting nucleus returns to its lowest energy state, emitting a high-energy photon in the process. [1]

The γ-radiation emitted from a radionuclide has a distinct energy, a kind of fingerprint to identify the nuclide. This is a key reason as to why radionuclides are used as tracers in different studies, e.g diffusion of an element, for monitoring blood flow inside a body, reaction kinetics. This is done by either ”labelling” a molecule, i.e substituting an atom in the molecule with a radioactive isotope of the same element to keep the chemical properties, or using the radionuclide by itself. Some radionuclides can also be used in cancer therapy, where the radiation is deposited into cancer cells, effectively killing them.

2.4 Analysis methods

2.4.1 Autoradiography

In autoradiography, a radioactive sample is placed on a photosensitive imaging plate under darkness. This exposes the plate to the γ-emissions from the sample, which are absorbed on the plate made of a semiconducting material where the radiation knocks out an electron, creating a hole. After exposure, the plate is analysed using a laser, which due to the heat generated, recombines the electrons and electron holes, which results in light being emitted. This gives a signal that is processed by a computer, resulting in a ”map” that resembles the radioactivity intensity of the sample. [15] This type of measurement is good for acquiring a visual representation of the distribution of radioactivity in a sample.

2.4.2 High-Purity Germanium, HPGe

High-purity Germanium detectors, HPGe, are used in γ-spectroscopy, i.e to detect, identify and quantify γ-radiation. The detectors are made of a semiconducting crystal, in this case of Germanium, which interacts with the incoming radiation. This radiation ionises atoms in the crystal, creating electron-hole pairs by exciting electrons from the valence band to the conducting band of the crystal. The amount

of electron-hole pairs created is proportional to the energy of the incoming radiation. By applying an electric field, the excited electrons and their respective electron holes will move to the electrodes, electrons towards the anode and holes to the cathode, producing an electric pulse that can be measured. The pulse contains information of the energy of the radiation, while the amount of pulses per unit of time shows the intensity of the radiation.

This pulse is sent to a computer where an analysis software converts the electric signal into a γ-spectrum showing the energy and intensity of the radiation detected by the crystal. From the obtained spectrum, different radionuclides can be identified, and their activity can be calculated if the instrument is calibrated against known sources. [15]

In this study, the activity from the 1173.2 keV γ-emission of ^{60}Co is used for all samples in order to keep the conditions and parameters as similar as possible between measurements. The measured activity can then be used to determine the diffusion of the radionuclide by calculating the relative specific activity compared to the source activity, corrected for the decay of ^{60}Co ($t_{1/2}$=5.3y) during the test period.

3

Method

3.1 Sample preparation

From the circular bentonite block, a sector was cut out around one of the ^{60}Co-sources, in this case the one oriented East. From this sector a part around the source of approximately 8 cm in each direction vertically was cut out, being the part most likely to contain the major amount of radioactivity. This piece was then cut into 8 vertical laminae with a thickness of approximately 20 mm.

The whole laminae were then analysed using autoradiography. This was done to get a good visual representation of the radioactivity and to possibly further narrow down where in the block the radioactivity was, thus decreasing the number of samples needed to be analysed in later steps.

The laminae would then subsequently be cut into smaller pieces of approx. 20 x 20 x 20 mm for radioactivity measurements. Between cutting and measuring, the laminae and the samples were placed in sealed plastic bags in an effort to as much as possible avoid the bentonite drying completely and thereby becoming more fragile and difficult to handle. The samples were labelled LXYZ, where X denotes the axial/vertical coordinate, Y the orbital/horizontal coordinate and Z the radial/horizontal coordinates, with X going from 1 to 8, Y from A to F and Z from 1 to 5, with 5 being the samples closest to the copper tube. A visualisation of how each lamina is divided can be seen in Figure 3.1.

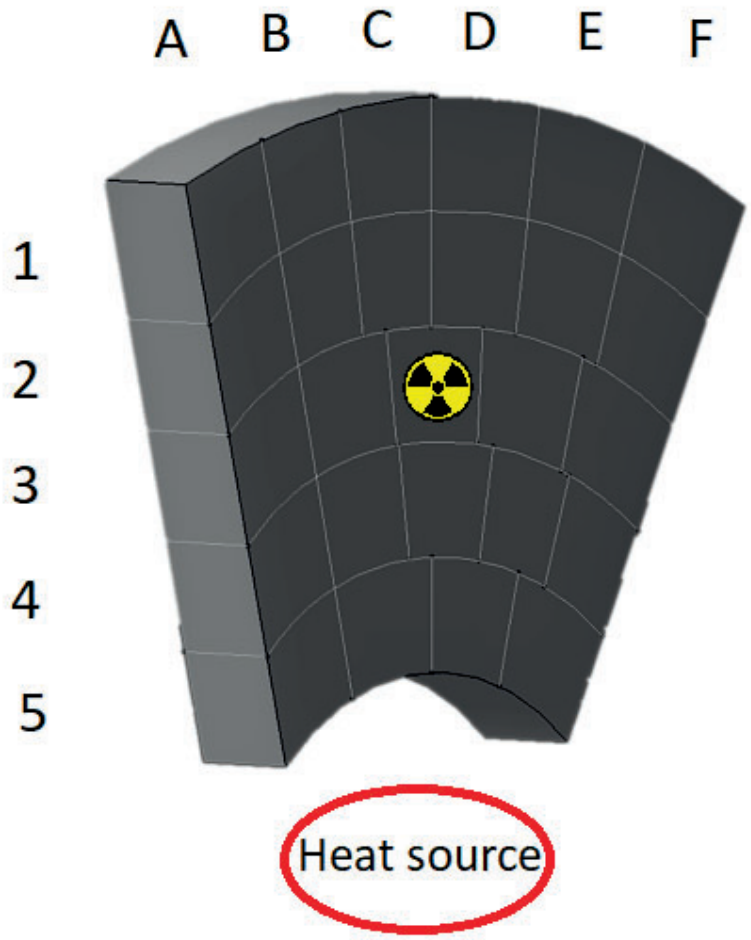

Figure 3.1: Visual representation of samples from a lamina with the naming system used for the samples included as well as the position of heat source and ^{60}Co-source (in lamina 4).

In order to cut the laminae into the smaller pieces, a Dremel multitool with a cutting disc was used. This resulted in some dust, but the cuts were clean and minimal fracturing was achieved. The samples were placed in separate plastic jars and weighed before and after drying in order to determine the water content of the bentonite. The samples were dried in a fume hood for two weeks before they were crushed to a fine powder in a stainless steel mortar.

3.2 Measurements

3.2.1 Autoradiography

The autoradiography was done by putting the laminae in plastic bags, and then onto an imaging plate for exposure. The imaging plate used in this analysis is a Fujifilm BAS TR-2025 imaging plate with high sensitivity. The exposure time was typically around 24h, but some samples were left for exposure over the weekend, resulting in approximately 70h of exposure. On each of the obtained radiograms, an inbuilt analysis tool was used to quantify the activity at different regions on each lamina. These regions were chosen at the approximately same position on all samples, and the background was chosen as a non-exposed corner of the photo plate in order to avoid any activity from the sample taken as background. Due to the difference in exposure time, the measured data was divided by total exposure time to obtain comparable results in order to draw any conclusions about the migration of ^{60}Co.

3.2.2 High-Purity Germanium, HPGe

After the samples had been crushed, they were weighed again before the plastic jars with lids (Brand) were put in sealed plastic bags. The measurements were done using a GEM23195 detector, 2002C preamplifier, DSA2000 multichannel analyzer, GammaAnalyst sample changer and Genie2000/APEX software (Canberra company, USA). The detector was efficiency calibrated with a mixed γ-source (TCC, Eckert & Ziegler, USA) mixed with 15g of pulverised bentonite. The HPGe detector with sample changer worked with one batch at a time, in this work one batch consists of the samples taken from one lamina, approximately 25 samples, meaning in total 8 batches are measured on the detector.

The live time and both the count rate and the activity for each sample were noted and logged in a spreadsheet for easy management. The activities were then divided by the sample mass in order to get the specific activity (Bq/g). The sample with the highest specific activity would be used as a reference value and was assumed to be the original position of the radioactive source. The ratio between the specific activities of the samples and the reference value were then plotted using MATLAB to obtain profiles showing how the specific activity changes with distance from the source. The specific activity as a function of distance from source would also be used in Equation 2.1 in order to obtain a value for the apparent diffusion of ^{60}Co that can be compared to earlier studies.

4

Results

4.1 Autoradiography

The 8 radiograms obtained from the autoradiography are shown in Appendix 1, and show a distinct difference in radioactivity between the different laminae, as well as within each lamina. From this, the original Co-source can be assumed to be within lamina 4 due to the high intensity visible, and also due to the activity measurements done within the autoradiography software. Also, there seems to be relatively low diffusion rate when taking lamina size and experiment time into account, since there is almost no activity in the opposite corner from the source on the same lamina. There does also seem to be higher activity registered in the lamina taken above the source as opposed to below (vertically in the bore hole). Otherwise the distribution seems to be symmetrical throughout.

4.2 Activity & Diffusion

The results from the radioactivity measurements are presented in Appendix 2, where the masses of the samples, the live time of the reactor and the total counts for ^{60}Co are presented, as well as the calculated specific activity (Bq/g). The sample with the highest specific activity is assumed to be the position of the source, with a specific activity of 2906.07 Bq/g. Using MATLAB, the relative specific activity was plotted to obtain diffusion profiles relative to the source sample. These profiles are shown in Figures 4.1 to 4.3 and correspond to orbital (x), radial (y) and axial (z) directions from the source, with the source as origin.

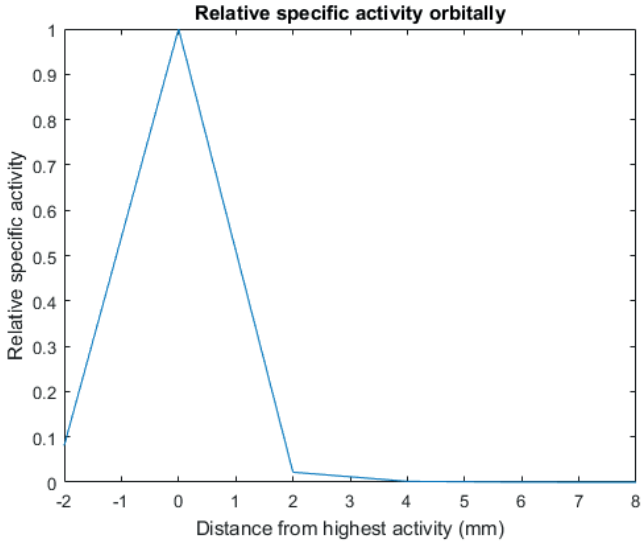

Figure 4.1: Diffusion profile orbitally (x)

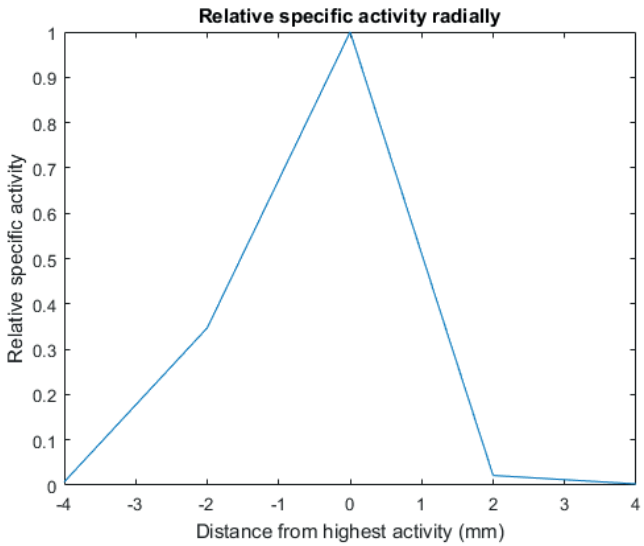

Figure 4.2: Diffusion profile radially (y)

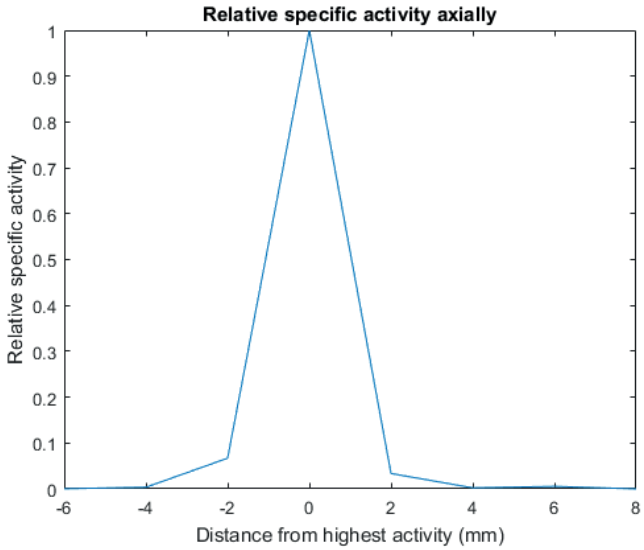

Figure 4.3: Diffusion profile axially(z)

From these profiles, together with the tables presented in Appendix 2, it becomes clear that the diffusion of ^{60}Co in bentonite is relatively slow, since the radioactivity decreases rapidly to background in just a few cm from the source. In the radial profile, there is a ”shoulder” towards the copper tube with the heater installed. This is expected due to the higher diffusivity at higher temperatures as previous studies have shown, see Table 2.1

Using Equation 2.1, the apparent diffusivity, D_a can be used as a fitting parameter for the solution by plotting the ratio between measured specific activity, C, and reference specific activity, C_0 from the source at the start of the experiment. By using the equation, the apparent diffusivity, D_a and the source radius, a, these parameters can be fitted to make the total error sum compared to the measured value as low as possible to ensure a good fit between the theoretical and actual values on the C/C_0 ratio. The C_0-values are corrected for the decay of ^{60}Co since the start of the experiment. Probably due to the difference between the different diffusion modes inside the bentonite, two curves are needed in order to obtain the best fitment to experimental data. The first curve corresponds to a slower path with stronger sorption, and the second curve to a faster path with weaker sorption.

The temperature profile inside the test package can be seen in Figure 4.4, ranging from 120^{o}C to 20^{o}C. However, the ^{60}Co-diffusion experiment is placed in the very bottom of the test package, where the temperature ranges from 90^{o}C to 60^{o}C from the copper tube outwards.

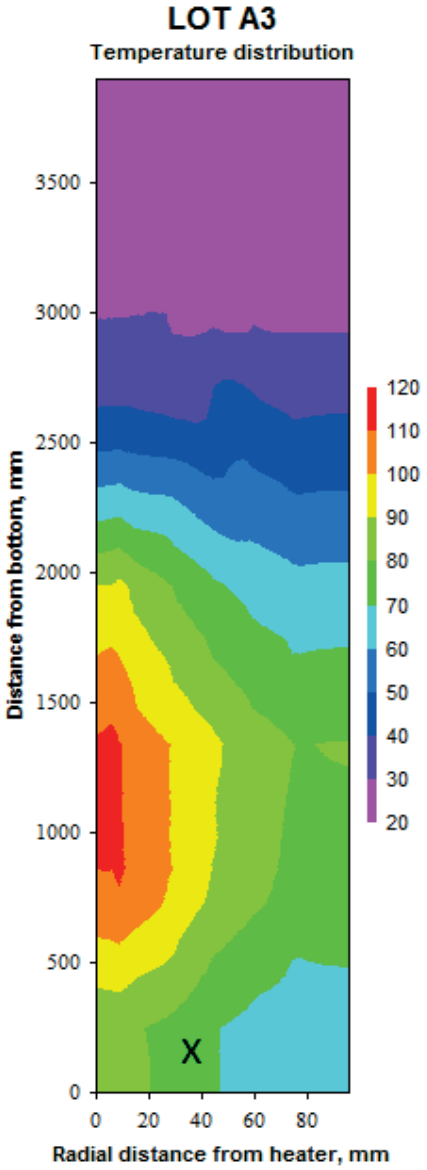

Figure 4.4: Temperature profile in LOT test package A3 with the approximate location of the ^{60}Co-source marked with an x

This temperature distribution means that the temperature dependent diffusivity was more easily evaluated by collecting the samples of each isotherm, that means samples from different laminae that have experienced the same temperature, out from the centre to the outer edge.

The results from the diffusion calculations of isotherms 2, 3 and 4, corresponding to temperatures of about 81^{o}C, 75^{o}C and 69^{o}C respectively, going from higher to lower temperature can be seen in Figures 4.5, 4.6 and 4.7 respectively. These isotherms are the main focus, since they are the ones with high enough activity to obtain good

results.

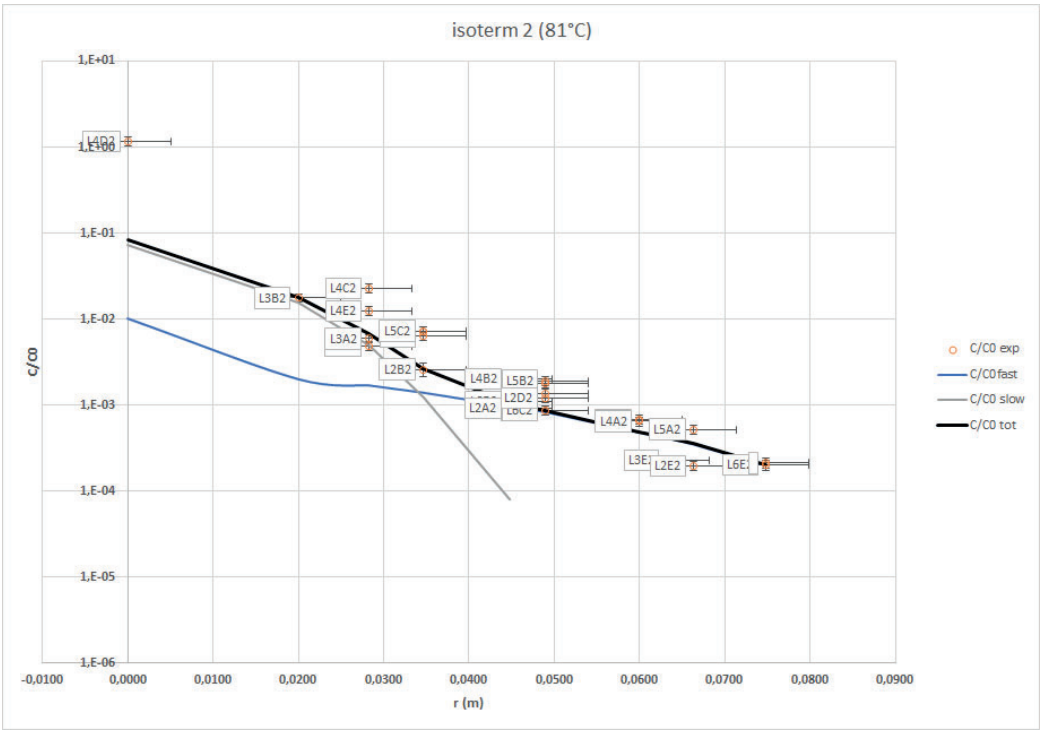

Figure 4.5: C/C_0 isotherm 2, 81^{o}C

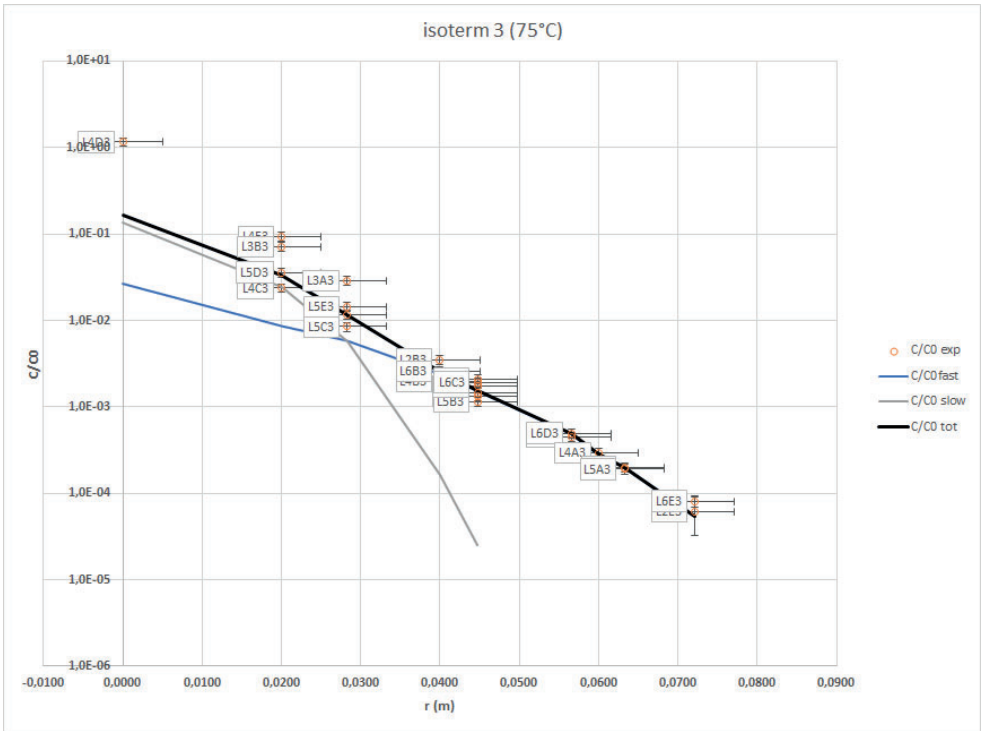

Figure 4.6: C/C_0 for isotherm 3, 75^{o}C

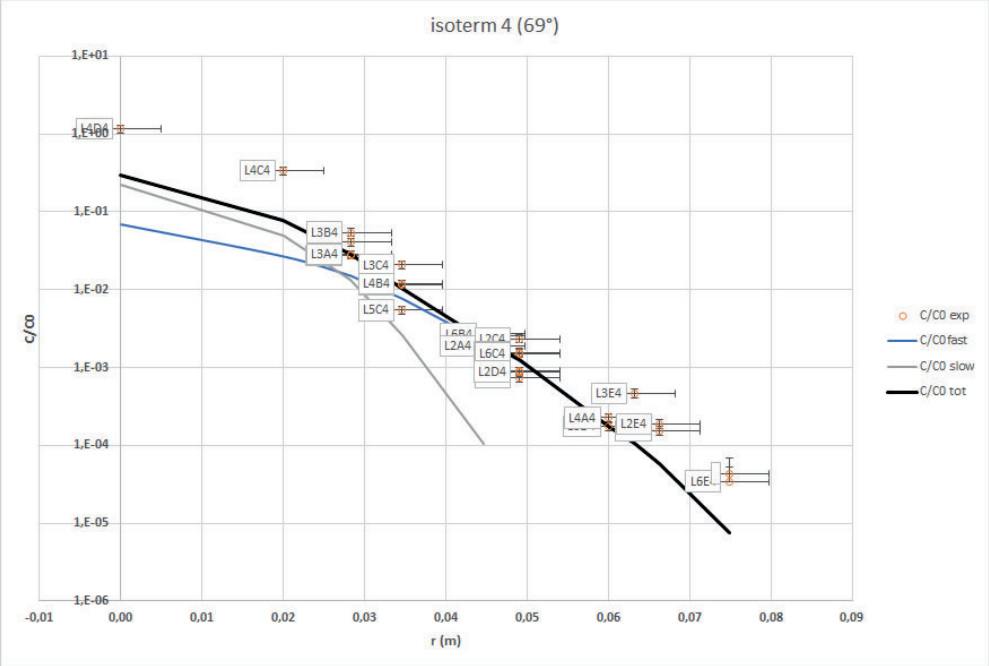

Figure 4.7: C/C_0 for isotherm 4, 69°C

In Table 4.1 the fitted D_a values for each isotherms are listed. These values are not far from those found in previous studies, especially at this temperature range (cf. Table 2.1). The apparent diffusivity is also higher at the isotherm with the higher temperature, which is also expected from the studies shown in Table 2.1. This shows that the proposed model for diffusion is consistent with the results from this study as well as for the earlier studies.

The obtained data clearly shows that there are two different diffusion profiles present in the bentonite clay. One is the interlayer diffusion (faster mode) which occurs within the clay particles, according to Appelo (2013). The other, slower, mode is the interparticle diffusion, between the particles. The difference in D_a for these modes probably comes from the mode of Co binding to the clay surface; the fast mode being ion-exchange and the slow mode being surface complexation. This is further supported by the temperature dependence on the fast mode, since ion-exchange is an entropy driven process, meaning that it is more sensitive to temperature change, as opposed to surface complexation.

Table 4.1: Apparent diffusivity for each isotherm.

Name	**D_a (slow) [m^2/s]**	**D_a (fast) [m^2/s]**	T [°C]
Isotherm 2	$9.61 \cdot 10^{-14}$	$8.78 \cdot 10^{-13}$	81
Isotherm 3	$6.75 \cdot 10^{-14}$	$3.44 \cdot 10^{-13}$	75
Isotherm 4	$7.19 \cdot 10^{-14}$	$2.17 \cdot 10^{-13}$	69

5

Discussion

Since the outermost part of the bentonite cylinder was drying more rapidly than anticipated, the mechanical stress from cutting it using a hand saw resulted in cracks and fractures. In order to keep the surface as intact as possible, the whole cylinder was covered by duct tape during the cutting process. There were however smaller pieces that broke loose, and were impossible to identify and put back in the correct place, meaning some laminae were smaller than others. This also occurred during the process of cutting the laminae into smaller samples, as well as a considerable amount of dust arising due to the multitool cutting disc. The arising dust may also be a source of cross-contamination between samples. The transfer of sample from mortar back to the jars also caused small losses of sample.

During the autoradiography, the different laminae did have some differences in exposure time, mainly the outermost laminae (with lowest activity) were exposed onto the imaging plate over the weekend in order to obtain a good result. The higher activity laminae were exposed for approximately 24h, since the high activity resulted in good radiograms after a shorter exposure time. Increasing this exposure time resulted in radiograms that were hard to analyse due to the high intensity, and lowering the exposure time for the low activity laminae resulted in the activity being almost non-discernible from the background. Due to the low diffusion rate as well as the 2cm thickness of the laminae, there could possibly be as much as 4cm between the surfaces exposed onto the imaging plate, resulting in a dramatic decrease of activity from one lamina to the next. The opposite could also be true, that the measured surface of one lamina is on the opposite side of the cut to the next lamina, meaning the same cross-section is measured twice.

From the measured data of specific radioactivity in the bentonite cubes, the diffusivity of ^{60}Co in bentonite is, as expected, low, and in line with previous studies. This further confirms that the chosen diffusion model corresponds well with the measurements taken from experiments with different time spans. In this study, two different diffusion paths in bentonite seems to be present and this may be the first time the two paths have been clearly resolved in an experiment. This is most probably due to the long time (19 years) that the experiment has been running. From the autoradiography, it is also clear that the radioactive Co is contained within a couple of centimetres from the original source, showing that the bentonite clay is effective as

backfill material that limits the diffusivity close to the Cu canisters in a final repository for used nuclear fuel. Some hot spots show up in the autoradiograms, such as in lamina 1, but the corresponding samples measured with HPGe show no real higher γ-activity than the surrounding samples, which most probably means that they were artefacts from contamination of another radionuclide or α-emissions, probably from Uranium daughters present in the bentonite, recorded by the imaging plate, showing higher intensity than what would be expected in that spot. The apparent higher intensity observed in the autoradiography of laminae above the source sample as opposed to below it could be due to the high temperature, and consequently higher diffusivity in the vertical direction. This finding from the autoradiography is mostly confirmed with the HPGe measurements, where in the radial profile (Fig. 4.2) had a marked shoulder in the direction of the heat source, however the axial profile (Fig. 4.3) had not. Furthermore, the evaluation of data by isotherms, which are layered approximately diagonally upwards towards the heat source (Fig. 4.4), show an increased diffusivity in that direction, which also supports this explanation.

There are however some samples where no activity was measured, even in laminae relatively close (a few cm) to the original source, which could mean that a longer measurement time could be used to obtain more counts, but this could also mean that the diffusion is too low, such that those samples does not actually contain any ^{60}Co or at least are at background activity.

6

Conclusion

From the results obtained in this study, there are two main modes of diffusion going on inside the bentonite clay, with different diffusivity. The faster mode is consistent with previous studies, meaning that the evaluated D_a values corresponds well to literary data from laboratory experiments, which is expected since the slower mode is not apparent in shorter-duration experiments. The faster mode, which is due to ion-exchange, and thus entropy-dependent is more sensitive to the temperature, as is expected. The diffusivity is higher closer to the copper tube containing the heater, which is also supported by earlier studies on temperature dependence of the diffusivity. The autoradiography together with the radioactivity measurements show that the distance inside the bentonite that the Co has diffused is very short, only a couple of centimetres, which also doesn't differ much from previous studies despite a high temperature. This together with the duration of the A3 test parcel experiment shows promising results for the use of bentonite clay as backfill material in a future KBS-3 final repository for used nuclear fuel.

References

[1] Gregory Choppin, Jan-Olov Liljenzin, Jan Rydberg, and Christian Ekberg. *Radiochemistry and Nuclear Chemistry*. Academic Press, Oxford, fourth ediition edition, 2013.

[2] International Atomic Energy Agency, IAEA. IAEA Power Reactor Information System, 2020.

[3] R. Ewing. The design and evaluation of nuclear-waste forms: Clues from mineralogy. *Canadian Mineralogist - CAN MINERALOG*, 39:697–715, 06 2001.

[4] SKB AB. SR-97 Post Closure Safety. I, 1999.

[5] Ola Karnland, Siv Olsson, Ann Dueck, Martin Birgersson, Ulf Nilsson, and Tania Hernan-håkansson. TR-09-29 Long term test of buffer material. (November), 2009.

[6] Encyclopedia Britannica. Bentonite, 2019.

[7] Stella Triantafyllou, Eirini Christodoulou, and Paraskevi Neou-Syngouna. Removal of nickel and cobalt from aqueous solutions by Na-activated bentonite. *Clays and Clay Minerals*, 47(5):567–572, 1999.

[8] D. Xu, D. D. Shao, C. L. Chen, A. P. Ren, and X. K. Wang. Effect of pH and fulvic acid on sorption and complexation of cobalt onto bare and FA bound MX-80 bentonite. *Radiochimica Acta*, 94(2):97–102, 2006.

[9] Ola Karnland, Torbjörn Sandén, Lars-Erik Johannesson, Trygve E Eriksen, Susanna Wold, Karsten Pedersen, Mehrdad Motamedi, and Bo Rosborg. TR-00-22 Long term test of buffer material. (December), 2000.

[10] James R. Welty, Charles E. Wicks, Robert E. Wilson, and Grewgory L. Rorrer. *Fundamentals of Momentum, Heat, and Mass Transfer*. John Wiley Sons, Inc, USA, 5th ed edition, 2008.

[11] C.A.J. Appelo. A review of porosity and diffusion in bentonite. (October),

2013.

[12] John Crank. *The Mathematics of Diffusion*. Clarendon Press, Oxford, 2nd ed edition, 1975.

[13] Mats Jansson, Trygve E. Eriksen, and Susanna Wold. LOT - in situ diffusion experiments using radioactive tracers. *Applied Clay Science*, 23(1-4):77–85, 2003.

[14] Mireia Molera Marimon. *On the sorption and diffusion of radionuclides in bentonite clay*. PhD thesis, Kungliga Tekniska Högskolan, 2002.

[15] Glenn F. Knoll. *Radiation Detection and Measurement*. John Wiley & Sons, New York, 2nd edition, 1989.

A

Appendix 1

A.1 Autoradiography

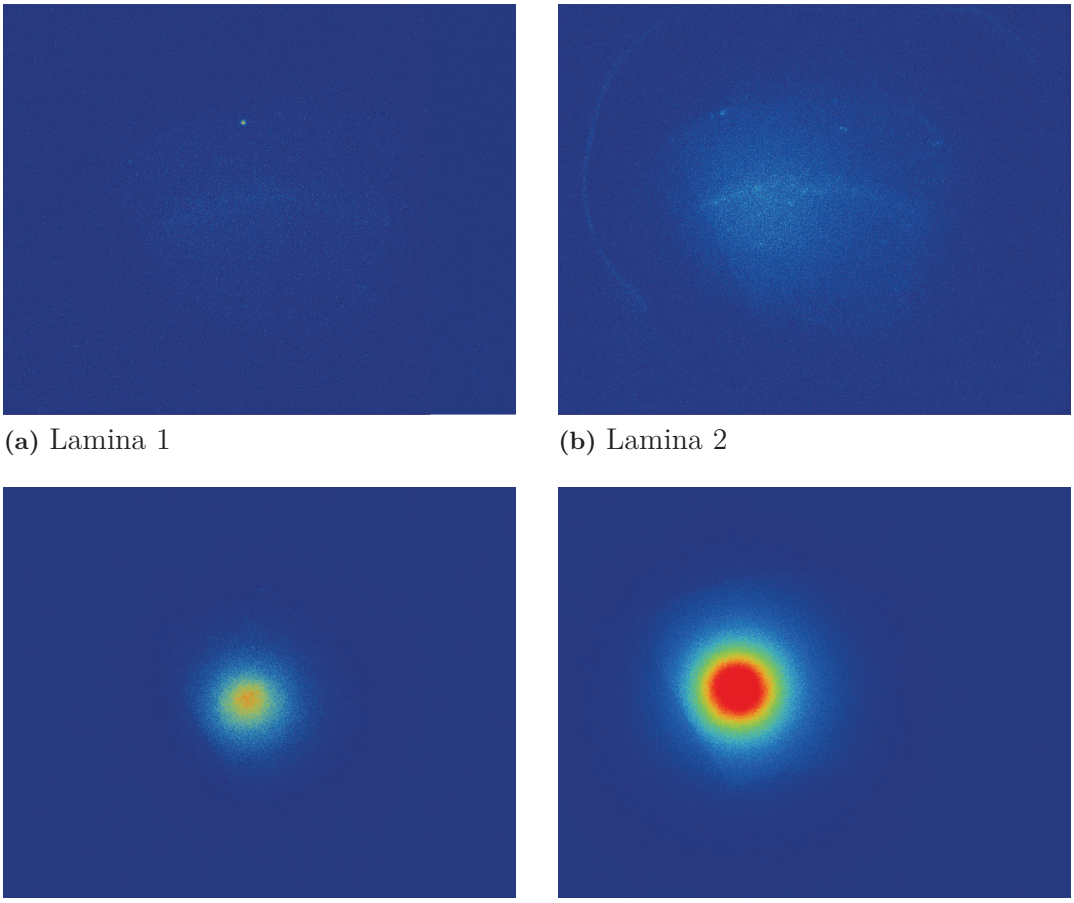

(a) Lamina 1 **(b)** Lamina 2

(c) Lamina 3 **(d)** Lamina 4

Figure A.1: The obtained radiograms for each lamina

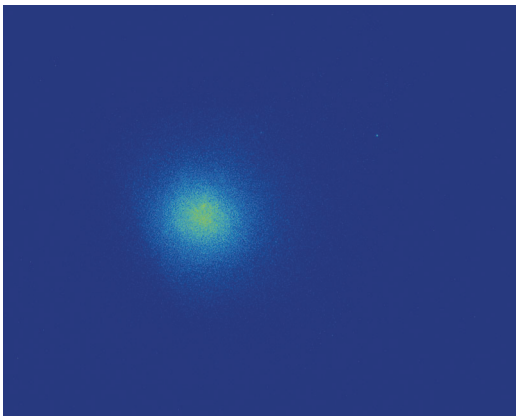

(a) Lamina 5

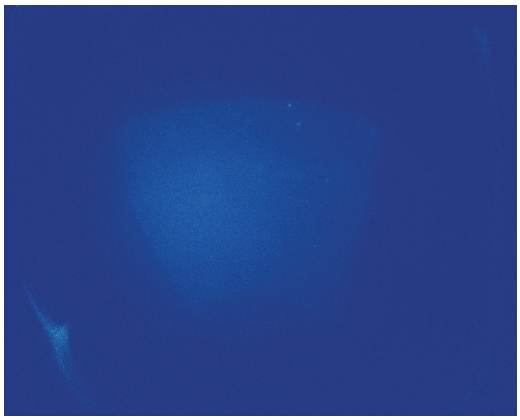

(b) Lamina 6

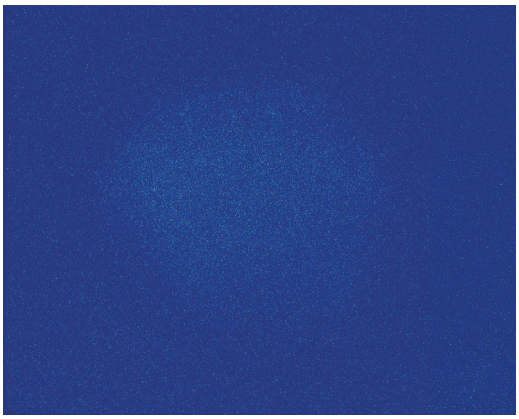

(c) Lamina 7

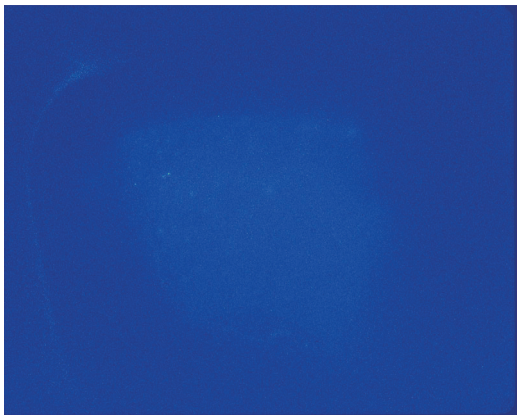

(d) Lamina 8

Figure A.2: The obtained radiograms for each lamina

B

Appendix 2

B.1 Radioactivity

Table B.1: Lamina 1

Name	Mass [g]	Counts	Live time [s]	Specific count rate [cps/g]	c/c_0
L1A1	13.4971	208	3606.5	0.00427304	0.000173517
L1B1	11.2475	228	3605.4	0.005622447	0.000228313
L1C1	10.2729	112	3605.4	0.003023928	0.000122794
L1D1	10.1602	112	3602.6	0.003059847	0.000124253
L1E1	6.7969	0	3607.1	0	0
L1F1	5.5657	15.6	3605.2	0.000777455	3.15705E-05
L1A2	9.1029	153	3602.2	0.00466599	0.000189474
L1B2	12.3018	339	3602.5	0.007649394	0.000310622
L1C2	10.3732	224	3601.5	0.005995865	0.000243477
L1D2	10.6051	147	3602.3	0.00384789	0.000156253
L1E2	9.3974	38	3610.1	0.0011201	4.54844E-05
L1F2	9.3311	16	3610	0.000474985	1.92879E-05
L1A3	12.5264	319	3609.1	0.007056112	0.000286531
L1B3	13.2247	403	3608.8	0.008444159	0.000342896
L1C3	12.0343	203	3616.8	0.004663916	0.00018939
L1D3	11.0554	46.3	3611.3	0.001159693	4.70921E-05
L1E3	11.2587	0	3603.5	0	0
L1A4	15.3837	241	3604.9	0.004345733	0.000176469
L1B4	16.4969	303	3604.4	0.005095741	0.000206925
L1C4	12.5296	76.1	3603.6	0.001685431	6.8441E-05
L1D4	11.5893	26	3601.7	0.000622886	2.52938E-05
L1E4	10.0261	0	3602.5	0	0
L1A5	16.3095	102	3603.5	0.001735541	7.04759E-05
L1B5	14.6476	78.6	3604.1	0.001488878	6.04595E-05
L1C5	12.7143	35.5	3605.5	0.000774409	3.14468E-05
L1D5	12.0569	0	3604.1	0	0

Table B.2: Lamina 2

Name	Mass [g]	Counts	Live time [s]	Specific count rate [cps/g]	c/c_0
L2A1	9.7664	534	3606.9	0.015159073	0.000615571
L2B1	12.6041	1090	3605.6	0.023984856	0.000973963
L2C1	13.6032	940	3605.6	0.019165018	0.000778242
L2D1	11.5544	376	3608.4	0.009018323	0.000366211
L2E1	12.5038	176	3607.5	0.003901794	0.000158442
L2F1	9.0405	40.3	3604.7	0.001236641	5.02168E-05
L2A2	11.6887	1320	3604.7	0.031328427	0.001272167
L2B2	11.6967	1980	3605.5	0.04695008	0.001906522
L2C2	11.7408	1730	3608.3	0.040836243	0.001658255
L2D2	13.151	722	3606.8	0.015221462	0.000618104
L2E2	9.9576	173	3609.7	0.004813049	0.000195446
L2F2	12.3305	86.1	3607.3	0.00193571	7.86042E-05
L2A3	7.9115	1380	3606.8	0.048361325	0.001963829
L2B3	13.6626	4310	3611.7	0.087343833	0.003546808
L2C3	12.2918	2170	3606.1	0.048956063	0.00198798
L2D3	14.789	509	3606	0.009544502	0.000387578
L2E3	12.8499	58.9	3607.5	0.001270601	5.15958E-05
L2A4	14.53	2840	3608.5	0.054165907	0.002199538
L2B4	14.2062	3210	3607.3	0.062639004	0.002543608
L2C4	15.2847	1130	3606.1	0.020501411	0.000832509
L2D4	12.4147	175	3607.1	0.003907902	0.00015869
L2E4	10.3826	24	3610.9	0.000640162	2.59953E-05
L2A5	13.4942	921	3619	0.018859228	0.000765825
L2B5	13.9225	905	3619.8	0.017957537	0.000729209
L2C5	13.7573	230	3618.3	0.004620512	0.000187627
L2D5	13.4584	67.6	3626.2	0.001385165	5.6248E-05

Table B.3: Lamina 3

Name	Mass [g]	Counts	Live time [s]	Specific count rate [cps/g]	c/c_0
L3A1	14.9449	2230	3601.9	0.041426687	0.001682231
L3B1	9.6453	2190	3602.3	0.063030173	0.002559493
L3C1	10.3482	1830	3604.6	0.049060187	0.001992208
L3D1	14.4848	1350	3605.5	0.025849715	0.00104969
L3E1	7.0003	188	3603.9	0.007451925	0.000302603
L3F1	5.0219	0	3601.6	0	0
L3A2	8.9293	5410	3602.5	0.168180586	0.00682938
L3B2	12.8839	13300	3604.4	0.28639888	0.01162992
L3C2	11.3737	5980	3602.6	0.145943034	0.00592637
L3D2	8.6167	1410	3603.2	0.045414002	0.001844146
L3E2	9.348	398	3605.3	0.011809267	0.000479544
L3F2	9.0279	138	3613.6	0.004230116	0.000171774
L3A3	9.8022	23500	3618	0.662637089	0.026907984
L3B3	12.6373	75500	3624	1.648558896	0.066943727
L3C3	9.7097	9410	3615	0.268086849	0.010886316
L3D3	12.9158	1570	3609.5	0.033676837	0.00136753
L3E3	10.5091	175	3611.5	0.004610892	0.000187236
L3A4	11.7565	20300	3618	0.477253835	0.019380048
L3B4	10.7212	24600	3617	0.634370824	0.025760164
L3C4	9.9027	4490	3615.8	0.125397338	0.005092063
L3D4	8.9249	581	3616.9	0.017998498	0.000730873
L3E4	8.8227	112	3602	0.003524299	0.000143113
L3A5	11.8746	3750	3603.6	0.087634618	0.003558616
L3B5	12.338	3660	3604.7	0.082293814	0.00334174
L3C5	10.2412	643	3605.7	0.017412877	0.000707092
L3D5	10.9015	109	3604.5	0.002773928	0.000112642

Table B.4: Lamina 4

Name	Mass [g]	Counts	Live time [s]	Specific count rate [cps/g]	c/c_0
L4A1	9.7459	2220	3602.3	0.063234071	0.002568
L4B1	13.0312	3290	3602.4	0.070084109	0.002846
L4C1	8.705	2210	3603.2	0.070458782	0.002861
L4D1	13.3904	1930	3603.8	0.039994758	0.001624
L4E1	11.9867	627	3604.4	0.014512256	0.000589
L4F1	7.9127	95.6	3605.3	0.003351134	0.000136
L4A2	8.2495	5100	3602.6	0.171603643	0.006968
L4B2	10.7867	20600	3604.9	0.529767605	0.021512
L4C2	9.0775	13400	3603.3	0.409673733	0.016636
L4D2	10.5375	4260	3601.4	0.112253697	0.004558
L4E2	11.9193	1100	3601.7	0.025623261	0.00104
L4F2	11.1971	208	3602.2	0.005156915	0.000209
L4A3	11.6263	83700	3619.2	1.989167476	0.080775
L4B3	13.8269	1330000	3906	24.62603997	1
L4C3	11.72	23000	3605.8	0.544250191	0.022101
L4D3	12.5336	2020	3602.7	0.044735	0.001817
L4E3	12.3762	286	3601.7	0.006416101	0.000261
L4A4	10.963	50900	3611.7	1.285513669	0.052201
L4B4	15.782	329000	3669.1	8.543776327	0.346941
L4C4	12.1634	42900	3609.1	0.977244844	0.039683
L4D4	14.5155	3220	3602.2	0.061582321	0.002501
L4E4	13.2137	512	3602.4	0.010756069	0.000437
L4A5	11.0852	6070	3605	0.151893745	0.006168
L4B5	11.3855	7350	3604.3	0.179107718	0.007273
L4C5	13.1039	1930	3604.2	0.040864657	0.001659
L4D5	13.0689	347	3602.2	0.007370936	0.000299

Table B.5: Lamina 5

Name	**Mass [g]**	**Counts**	**Live time [s]**	**Specific count rate [cps/g]**	**c/c_0**
L5A1	8.5248	2220965	3601-5	0.031431	0.001276
L5B1	11.827	1950	3601.8	0.045776	0.001859
L5C1	9.43	1530	3603.5	0.045025	0.001828
L5D1	10.4446	929	3602.9	0.024687	0.001002
L5E1	9.7157	341	3613.8	0.009712	0.000394
L5F1	11.4808	123	3614.7	0.002964	0.00012
L5A2	7.5738	2510	3604.2	0.09195	0.003734
L5B2	10.6626	6540	3604.7	0.170155	0.00691
L5C2	10.1404	5030	3603.6	0.13765	0.00559
L5D2	11.3638	2400	3604.1	0.058599	0.00238
L5E2	13.6198	956	3603.2	0.01948	0.000791
L5F2	12.7344	226	3603.1	0.004926	0.0002
L5A3	13.9686	16800	3607.8	0.33336	0.013537
L5B3	11.5273	34400	3611.8	0.826242	0.033552
L5C3	12.8459	9070	3607.8	0.195704	0.007947
L5D3	12.673	1210	3605.6	0.026481	0.001075
L5E3	14.2045	200	3605.1	0.003906	0.000159
L5A4	11.4173	11400	3603.6	0.27708	0.011251
L5B4	11.3705	27000	3606.3	0.658449	0.026738
L5C4	12.3027	12900	3604.2	0.290925	0.011814
L5D4	15.9446	2070	3604.7	0.036015	0.001462
L5E4	14.0897	226	3604	0.004451	0.000181
L5A5	11.1966	2550	3602.3	0.063223	0.002567
L5B5	10.8062	3000	3602.1	0.077071	0.00313
L5C5	14.4045	1110	3601.7	0.021395	0.000869
L5D5	13.423	152	3602.1	0.003144	0.000128

Table B.6: Lamina 6

Name	Mass [g]	Counts	Live time [s]	Specific count rate [cps/g]	c/c_0
L6A1	7.7615	335	3603	0.011979395	0.000449913
L6B1	9.2768	612	3604.3	0.018303422	0.000687426
L6C1	9.2106	479	3604.6	0.014427481	0.000541856
L6D1	11.5767	386	3605	0.009249053	0.000347369
L6E1	10.5781	147	3604.9	0.00385493	0.00014478
L6F1	10.2047	37.7	3606.2	0.001024451	3.84755E-05
L6A2	8.1582	576	3605.8	0.019580623	0.000735394
L6B2	6.5601	466	3606.8	0.019694883	0.000739685
L6C2	8.3712	842	3606.1	0.027892446	0.001047563
L6D2	7.9727	418	3604.9	0.014543791	0.000546224
L6E2	10.8608	196	3601.5	0.005010843	0.000188193
L6F2	8.2392	44.8	3601.5	0.001509766	5.67026E-05
L6A3	11.2973	1600	3601.6	0.03932329	0.001476873
L6B3	10.065	2170	3602.4	0.059848603	0.002247747
L6C3	9.4716	1530	3603.3	0.044829889	0.001683686
L6D3	17.728	724	3602.1	0.01133765	0.000425811
L6E3	13.7663	101	3602.3	0.002036687	7.64923E-05
L6A4	12.5042	1600	3603.4	0.035510076	0.00133366
L6B4	13.0405	2060	3603	0.043843853	0.001646653
L6C4	10.8128	757	3603	0.019430924	0.000729771
L6D4	9.4995	175	3602	0.005114387	0.000192082
L6E4	9.0979	27.2	3601.8	0.000830057	3.11746E-05
L6A5	11.2651	549	3601.6	0.013531371	0.000508201
L6B5	11.7028	639	3601.1	0.015162677	0.000569468
L6C5	10.706	200	3600.8	0.005188045	0.000194849
L6D5	11.3619	68.6	3601.8	0.001676307	6.29574E-05

Table B.7: Lamina 7

Name	Mass [g]	Counts	Live time [s]	Specific count rate [cps/g]	c/c_0
L7A1	14.4578	295	3604.7	0.004088384	0.000166019
L7B1	10.4497	24	3602	0.000420578	1.70786E-05
L7C1	7.4426	53	3602	0.001113646	4.52223E-05
L7D1	8.9656	131	3603.7	0.002520089	0.000102334
L7E1	9.4157	241	3602.3	0.004449435	0.00018068
L7A2	16.6882	328	3601.9	0.00405995	0.000164864
L7B2	9.4698	51.1	3601.9	0.00093926	3.81409E-05
L7C2	13.5553	0	3602.7	0	0
L7D2	11.4668	180	3601.9	0.002944995	0.000119589
L7E2	8.7875	280	3602.6	0.005351735	0.00021732
L7A3	15.7879	268	3602.7	0.003485405	0.000141533
L7B3	11.7568	175	3602.9	0.00281083	0.000114141
L7C3	10.6003	0	3602.8	0	0
L7D3	12.3071	135	3602.9	0.002075407	8.42769E-05
L7E3	13.3009	54.8	3602.4	0.000804489	3.26682E-05
L7A4	13.1999	124	3602.5	0.001837105	7.46001E-05
L7B4	12.4072	96.2	3601.8	0.001466594	5.95546E-05
L7C4	10.3757	34.3	3611.1	0.0005961	2.42061E-05
L7D4	10.8858	0	3608.2	0	0

Table B.8: Lamina 8

Name	Mass [g]	Counts	Live time [s]	Specific count rate [cps/g]	c/c_0
L8A1	-	-	-	-	-
L8B1	14.0192	0	3601.8	0.00E+00	0.00E+00
L8C1	8.9674	27.9	3601.4	8.64E-04	3.51E-05
L8D1	9.8391	60.5	3601.4	1.71E-03	6.93E-05
L8E1	9.1686	55.1	3601.9	1.67E-03	6.78E-05
L8F1	7.7476	0	3601.8	0.00E+00	0.00E+00
L8A2	6.6495	0	3601.5	0.00E+00	0.00E+00
L8B2	9.7721	19.2	3602.4	5.45E-04	2.21E-05
L8C2	8.9184	26	3601.9	8.09E-04	3.29E-05
L8D2	8.9241	54.5	3601.1	1.70E-03	6.89E-05
L8E2	10.9869	42.3	3601.1	1.07E-03	4.34E-05
L8F2	9.3367	26.3	3601.2	7.82E-04	3.18E-05
L8A3	9.1418	0	3601.9	0.00E+00	0.00E+00
L8B3	9.0827	0	3602	0.00E+00	0.00E+00
L8C3	10.8809	26.5	3604.7	6.76E-04	2.74E-05
L8D3	14.7718	61	3604.4	1.15E-03	4.65E-05
L8E3	17.8075	31	3603.6	4.83E-04	1.96E-05
L8A4	12.0981	0	3605.2	0.00E+00	0.00E+00
L8B4	13.8677	0	3603.4	0.00E+00	0.00E+00
L8C4	15.0404	23.2	3602	4.28E-04	1.74E-05
L8D4	11.0899	25.2	3602.1	6.31E-04	2.56E-05
L8E4	11.2986	12.1	3602.5	2.97E-04	1.21E-05
L8A5	12.4249	0	3601.2	0.00E+00	0.00E+00
L8B5	11.5538	0	3602	0.00E+00	0.00E+00
L8C5	10.1043	0	3608.3	0.00E+00	0.00E+00
L8D5	10.8156	0	3602.2	0.00E+00	0.00E+00